Nanoscale Advances

ROYAL SOCIETY OF CHEMISTRY

PAPER

View Article Online
View Journal | View Issue

Cite this: *Nanoscale Adv.*, 2021, **3**, 3159

A new strategy for large-scale synthesis of $Na_{0.5}Bi_{0.5}TiO_3$ nanowires and their application in piezocatalytic degradation†

Rui Huang, Jiang Wu, * Enzhu Lin, Zihan Kang, Ni Qin * and Dinghua Bao

Received 10th January 2021
Accepted 1st April 2021

DOI: 10.1039/d1na00024a

rsc.li/nanoscale-advances

Developing new techniques that can synthesize one-dimensional piezoelectric materials on a large scale is of great significance for boosting piezocatalytic applications. In this work, we proposed a high-efficiency template hydrothermal method for large-scale synthesis of piezoelectric $Na_{0.5}Bi_{0.5}TiO_3$ (NBT) nanowires. By ion-exchange with Bi^{3+}, $Na_2Ti_3O_7$ template nanowires can be easily and entirely transformed to NBT. The piezocatalytic activity of the NBT nanowires was thoroughly investigated with respect to their capability to degrade typical organic pollutants, including Rhodamine B, methylene blue, methyl orange, tetracycline hydrochloride, phenol, and bisphenol A. The NBT nanowires exhibited the highest efficiency in piezocatalytic degradation of Rhodamine B, which was completely decomposed within 80 min (rate constant ~0.0575 min^{-1}). The electron spin resonance spin-trapping technique and active species capture experiments were employed to characterize free radicals. The present work is advantageous for the high yield of NBT nanowires and the excellent piezocatalytic performance. The reported template hydrothermal method can potentially be extended to the synthesis of other perovskite nanowires.

Introduction

With the rapid development of industrialization, environmental water contamination has become increasingly prominent.[1,2] Various advanced oxidation processes (AOPs)[3] such as the Fenton reaction,[4] photolysis,[5] photocatalysis[6] and processes based on ozone[7] have been developed to remove organic compounds from wastewater. As a novel AOP technology with cost-competitive and environmentally friendly properties, piezocatalysis has received widespread attention.[8] A typical piezocatalytic process usually adopts a piezoelectric material in powder form as the piezocatalyst. When a varying mechanical force is applied to the piezocatalyst, a polarization field will be generated in the piezocatalyst. The polarization field can lead to separation of free charges and production of reactive oxygen species (ROS) through redox reactions.[9]

Representative piezocatalysts include $BaTiO_3$,[10] $Pb(Zr_{0.52}Ti_{0.48})O_3$,[11] $Pb(Mg_{1/3}Nb_{2/3})O_3$–$x$$PbTiO_3$,[12] Bi_2WO_6,[13] $KNbO_3$,[14] and $NaNbO_3$,[15] which have been proved to be effective in degrading various organic pollutants. Unfortunately, most of the reported piezocatalysts suffer from low efficiency in actual applications. Much effort has been devoted to improving the functional performance of piezocatalysts. It is generally believed that the large piezo-electric coefficient, highly flexible structure and abundant active sites of piezocatalysts are beneficial. More recently, electrical conductivity was regarded as another vital factor that influenced the piezocatalytic performance.[16–19] It was suggested that the high electrical conductivity helped to accelerate charge transfer in the piezocatalytic process and thus enhanced the piezocatalytic activity.[20]

$Na_{0.5}Bi_{0.5}TiO_3$ (NBT) is an attractive piezoelectric material because of its large piezoelectric coefficient (d_{33} value of ~58 pC N^{-1})[21,22] and high Curie temperature (340 °C).[23] In addition, it is reported that the relatively high electrical conductivity (~10^{-5} S m^{-1}) of NBT may be favorable for piezocatalytic applications.[20] Recently, research studies on the piezocatalytic performance of NBT have been carried out.[24–26] It is worth noting that most of the reported NBT piezocatalysts are microparticles[24] or multi-crystalline nanofibers.[25] The piezocatalytic performance of NBT single-crystalline nanowires has never been reported. It is highly expected that single-crystalline nanowires may have higher piezocatalytic activity because of their higher flexibility and larger specific surface area.

In this work, NBT single-crystalline nanowires with uniform morphology were prepared *via* a template hydrothermal method using $Na_2Ti_3O_7$ nanowires as the template. The piezocatalytic activity of the NBT nanowires was evaluated from the degradation efficiency for different kinds of organic pollutants. Piezocatalytic mechanisms were also systematically investigated through quenching experiments and ESR characterization. This study may open up a promising approach to design

State Key Laboratory of Optoelectronic Materials and Technologies, School of Materials Science and Engineering, Sun Yat-Sen University, Guangzhou 510275, China. E-mail: wujiang1990@126.com; qinni2@mail.sysu.edu.cn

† Electronic supplementary information (ESI) available. See DOI: 10.1039/d1na00024a

and synthesize piezoelectric nanowires for environmental purification.

Experimental section

Preparation of $Na_{0.5}Bi_{0.5}TiO_3$ nanowires

NBT nanowires were synthesized based on a template hydrothermal reaction. The first step in the reaction is to synthesize $Na_2Ti_3O_7$ nanowires,[27] which act as the titanium precursor for the NBT nanowires. First, 1.5974 g of TiO_2 was dispersed in 70 mL of 10 mol L^{-1} NaOH solution. The mixed solution was then sealed in a 100 mL Teflon-lined stainless-steel autoclave and heated at 240 °C for 24 h. Following this reaction, the resulting $Na_2Ti_3O_7$ nanowires were washed by repeated centrifugation with DI water, until the pH reached around 7. Finally, the product was dried at 70 °C for 12 h.

The NBT nanowires were subsequently synthesized through a hydrothermal reaction, in which the prepared $Na_2Ti_3O_7$ nanowires were employed as a Ti^{4+} source and $Bi(NO_3)_3\cdot 5H_2O$ was employed as a Bi^{3+} source. First, 0.4851 g of $Bi(NO_3)_3\cdot 5H_2O$ and 0.2010 g of $Na_2Ti_3O_7$ were dispersed in NaOH solution. The mixed solution was then sonicated for 20 min and stirred for 30 min to form a uniform suspension. The final mixture was hydrothermally treated at 200–240 °C for 6–24 h in a 100 mL Teflon-lined stainless-steel autoclave with a 70% filling factor. The reaction temperature, reaction time, and mineralizer concentration for the synthesis of pure NBT nanowires were investigated in detail. After the reaction, the formed white precipitate was collected by centrifugation, washed several times with distilled water and 0.2 mol L^{-1} acetic acid, and finally dried at 60 °C for 12 h.

Characterization

X-ray diffraction (XRD, Rigaku D/MAX 2200 VPC) with Cu Kα1 radiation was employed to investigate the structure of the crystalline samples. The morphology of the samples was observed by field-emission scanning electron microscopy (SEM, Hitachi SU8010). Energy dispersive spectroscopy mapping (EDS-mapping) was carried out using a Zeiss G500 equipped with an energy spectrum analyzer. High resolution transmission electron microscopy (HRTEM) investigations were performed using a JEOL JEM-2100 TEM (with an acceleration voltage of 200 kV). X-ray photoelectron spectroscopy (XPS) was carried out using a high-performance electron spectrometer (Thermo Scientific ESCALAB 250Xi) with an Al Kα X-ray source. All binding energies were calibrated using the C 1s peak with a fixed value of 284.8 eV.

Piezocatalytic activity test

The piezocatalytic ability of the prepared NBT samples was systematically evaluated from the degradation of Rhodamine B (5 mg L^{-1}) under ultrasonic vibration (80 W, ~40 kHz). In a typical piezocatalytic experiment, 0.1 g NBT sample was added into a 100 mL solution of organic pollutants. Prior to the ultrasonic vibration, the suspension was magnetically stirred in the dark for 30 min to reach the adsorption–desorption equilibrium between NBT and the pollutants. The temperature of the piezocatalytic reaction system was kept at room temperature (25 °C) by using a water cooling circulation system. During the whole degradation process, 4 mL of the suspension was collected and centrifuged to remove the catalysts. The ultraviolet-visible (UV-vis) absorption spectrum of the supernatant was analyzed using a Shimadzu UV-3600 spectrophotometer. Furthermore, methylene orange (MO, 5 mg L^{-1}), methylene blue (MB, 5 mg L^{-1}), bisphenol A (BPA, 5 mg L^{-1}), tetracycline hydrochloride (TH, 5 mg L^{-1}), and phenol (5 mg L^{-1}) were also employed to evaluate the piezocatalytic activity of NBT nanowires.

Detection of free radicals

In situ capture experiments were conducted to investigate the active species generated in the piezocatalytic process. Specifically, 2 mmol L^{-1} disodium ethylene diamine tetra-acetate dehydrate (EDTA-2Na), 10 mmol L^{-1} *tert*-butyl alcohol (TBA), and 0.15 mmol L^{-1} benzoquinone (BQ) were employed as scavengers for holes (h^+), hydroxyl radicals ($\cdot OH$) and superoxides ($\cdot O_2^-$), respectively.

Furthermore, the electron spin resonance (ESR) technique was also employed to detect active free radicals such as radical $\cdot OH$ and radical $\cdot O_2^-$ with the assistance of 5,5-dimethyl-1-pyrroline N-oxide (DMPO). ESR investigations were conducted on a Bruker A300-10-12 spectrometer. Specifically, for the detection of radical $\cdot OH$, the as-prepared sample was dispersed in deionized water, and for the detection of radical $\cdot O_2^-$, the as-prepared sample was dispersed in dimethyl sulphoxide (DMSO).

Results and discussion

In hydrothermal synthesis, the properties of precursors have a major effect on the morphology of the products. Commonly used Ti precursors, including tetrabutyl titanate,[28] titanium dioxide,[29] and titanium tetrachloride,[30] often lead to the formation of coarse agglomerated particles because of their low solubility or hydrolysis properties.[31] The layered titanate $Na_2Ti_3O_7$ emerged as a great substitute for these precursors. The crystal structure of $Na_2Ti_3O_7$ is composed of TiO_6 octahedra, which are joined by corners and edges to form a zig–zag structure, with rectangular tunnels along the *z*-axis. The open-layered structure of $Na_2Ti_3O_7$ is favorable for topochemical transformation.[32] In our previous work,[33] $Na_2Ti_3O_7$ was employed as the template for growing bismuth titanate under hydrothermal conditions. A similar process was adopted in this work to synthesize NBT nanowires.

Fig. 1 schematically depicts the processing steps for growing NBT nanowires. In the first step, $Na_2Ti_3O_7$ nanowires were prepared *via* a simple hydrothermal method. In the following step, $Na_2Ti_3O_7$ and $Bi(NO_3)_3\cdot 5H_2O$ were added to NaOH solution. During the reaction, Bi^{3+} ions will reduce the stability of the layered titanate $Na_2Ti_3O_7$ and break the connection between the TiO_6 octahedra.[34] The dissociated TiO_6 octahedra will then react with Bi^{3+} and Na^+ ions to form perovskite-type NBT.

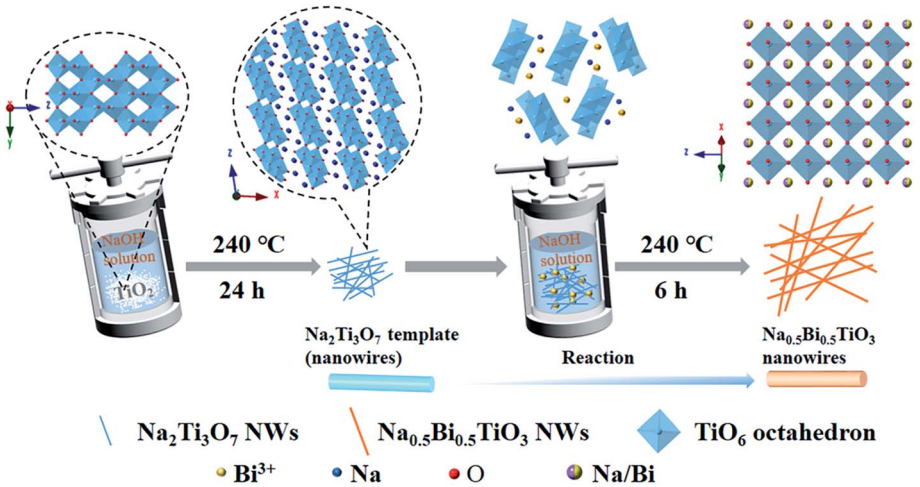

Fig. 1 Schematic of the formation mechanisms of $Na_{0.5}Bi_{0.5}TiO_3$ nanowires.

The XRD pattern of the synthesized $Na_2Ti_3O_7$ nanowires is shown in Fig. S1,† which demonstrates that pure-phase $Na_2Ti_3O_7$ (JCPDS No. 31–1329) has been formed. Fig. 2a–c show the XRD patterns of the NBT samples prepared under different reaction conditions. As shown in Fig. 2a, a composed phase structure was obtained in the samples synthesized at lower NaOH concentrations (3–5 mol L^{-1}). The major phase can be identified as NBT with a monoclinic or pseudo hexagonal structure (JCPDS No. 46-0001), and the additional peaks can be ascribed to $Na_5Bi_{4.5}Ti_4O_{15}$. When increasing the NaOH concentration to 10 mol L^{-1}, the secondary phase disappeared completely, and pure-phase NBT was obtained. Fig. 2b illustrates the influence of reaction temperature (200–240 °C) on the phase constitution of the product. The NaOH concentration was 10 mol L^{-1}. In the synthesis at 200 °C for 24 h, the NBT phase was formed along with $Na_2Ti_3O_7$ and Bi_2O_3 secondary phases. The pure-phase product was obtained by increasing the reaction temperature to over 220 °C. Based on these results, one may conclude that the high mineralizer concentration and high reaction temperature are beneficial for the hydrothermal synthesis of NBT. We found that the reaction time (6 h to 24 h) has little influence on the phase constitution of the hydrothermal product (Fig. 2c). For the NBT samples synthesized after 12 hours (NBT-12), the peak intensity of (110) and (220) was slightly enhanced, which may be due to the fact that the NBT-12 samples were a mixture of nanobelts and nanoparticles

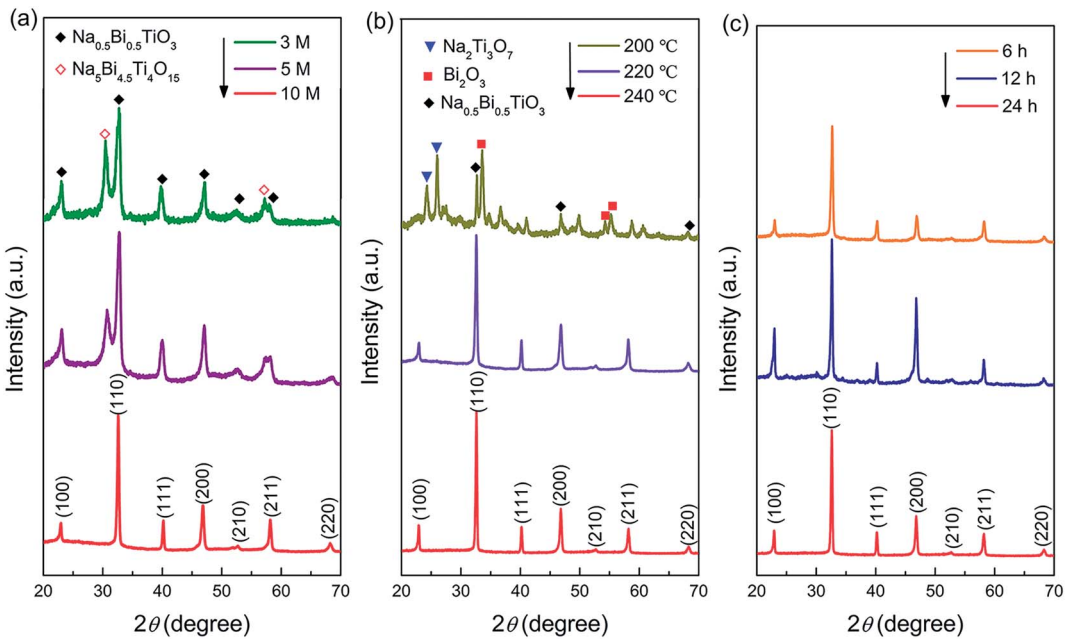

Fig. 2 XRD patterns of the $Na_{0.5}Bi_{0.5}TiO_3$ samples prepared at (a) different NaOH concentrations (3–10 mol L^{-1}, 240 °C, 24 h), (b) different reaction temperatures (200–240 °C, 10 mol L^{-1}, 24 h), and (c) different reaction times (6–24 h, 240 °C, 10 mol L^{-1}).

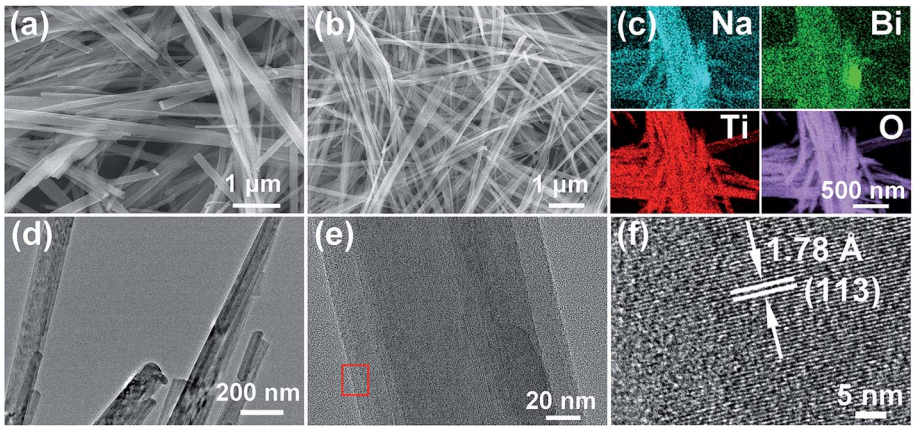

Fig. 3 SEM images of (a) $Na_2Ti_3O_7$ and (b) $Na_{0.5}Bi_{0.5}TiO_3$ nanowires; (c) EDS mapping, (d and e) TEM, and (f) HRTEM of $Na_{0.5}Bi_{0.5}TiO_3$ nanowires.

(Fig. S2†). The larger area of nanobelts results in the (100) and (200) facets being more easily scanned by X-ray. The NBT samples obtained from the 24 h-synthesis are crystallized into micro-scale particles (Fig. S3†). Pure-phase NBT nanowires were finally obtained by reducing the hydrothermal reaction time to 6 h.

The morphology of the pure-phase NBT nanowires can be clearly observed by SEM. Fig. 3a shows the SEM image of the $Na_2Ti_3O_7$ template nanowires, which are straight and smooth with an average lateral dimension of ~250 nm and a longitude larger than 5 μm. After reacting with $Bi(NO_3)_3$ solution, the $Na_2Ti_3O_7$ template nanowires were entirely transformed to uniform and slender NBT nanowires (Fig. 3b). The lateral dimension of the nanowires is about 100 nm. The distribution of elements in the NBT nanowires was analyzed by the EDX spectroscopy elemental mapping technique. As shown in

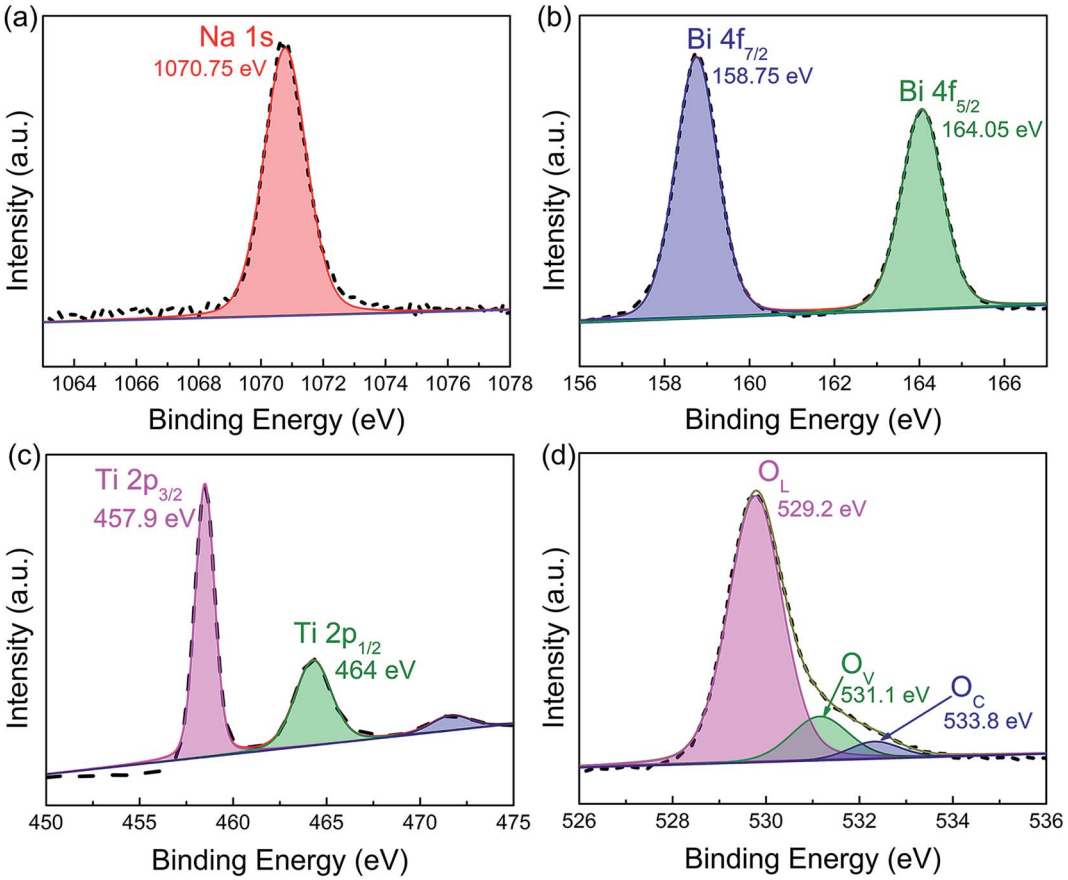

Fig. 4 High-resolution XPS spectra of the as-prepared $Na_{0.5}Bi_{0.5}TiO_3$ nanowires: (a) Na 1s, (b) Bi 4f, (c) Ti 2p, and (d) O 1s.

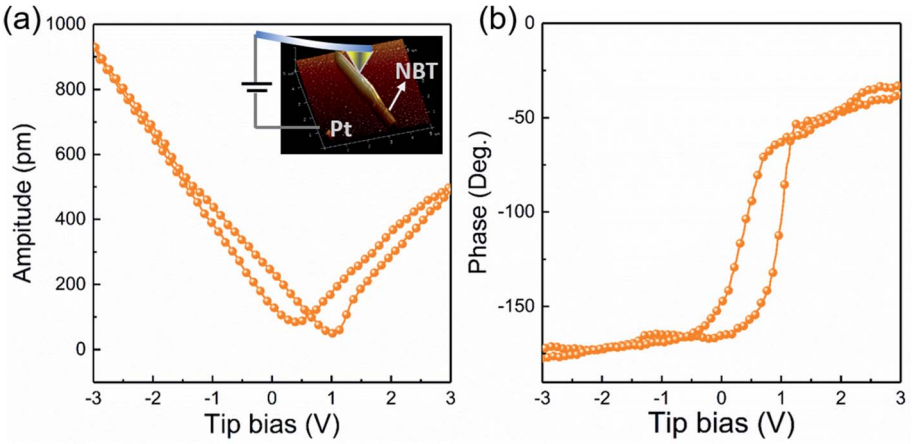

Fig. 5 (a) Amplitude butterfly curve (the inset: experimental setup of PFM) and (b) phase hysteresis of NBT NWs.

Fig. 3c, all the involved elements (Bi, Na, Ti, and O) are homogeneously distributed and well-matched with each other. The analytical composition of the obtained $Na_{0.5}Bi_{0.5}TiO_3$ was characterized using EDS spectra (Fig. S4†), in which the ratio of Na, Bi, and Ti in NBT nanowires is 22.2 : 22.8 : 55. The TEM images (Fig. 3d–e) illustrate the straight and smooth surface of

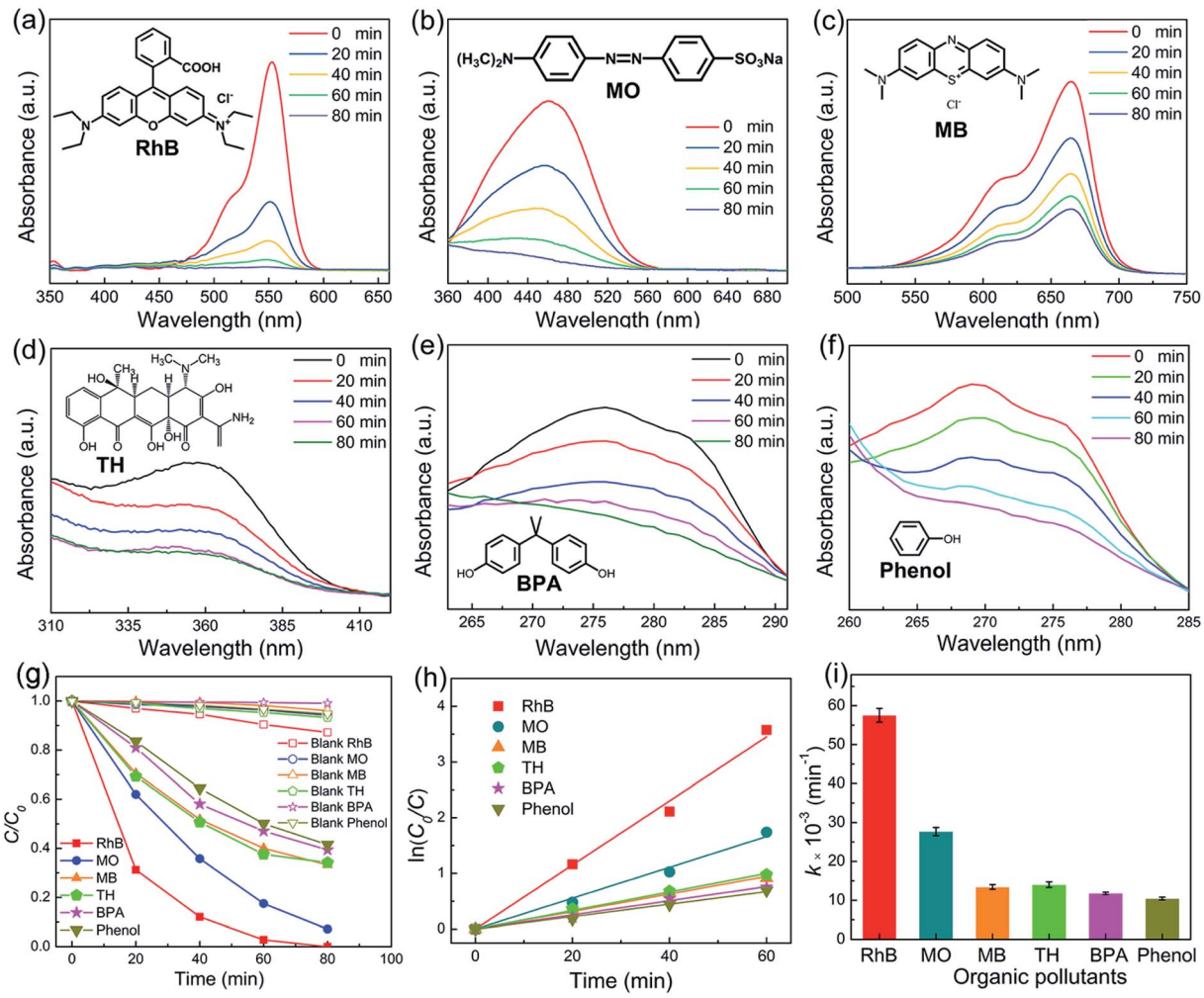

Fig. 6 Temporal absorption spectra of (a) RhB, (b) MO, (c) MB, (d) TH, (e) BPA and (f) phenol degraded by $Na_{0.5}Bi_{0.5}TiO_3$ nanowires under ultrasonic vibration. (g) Piezocatalytic degradation dynamic curves, (h) plots of $\ln(C_0/C)$ *versus* time, and (i) first-order rate constants of piezocatalytic degradation of different contaminants.

Table 1 Summary of NBT materials reported earlier along with their piezocatalytic performance

Synthesis method	Morphology	Degradation rate (min^{-1})	References
Hydrothermal	Micron cube	4.36×10^{-3}	37
Electrospinning	Nanofiber	$\sim 12 \times 10^{-3}$	38
Hydrothermal	Nanosphere	$\sim 35 \times 10^{-3}$	20
Hydrothermal	Nanowire	57.5×10^{-3}	This work

the NBT nanowires, indicating the high-quality of the present material. The amplified HRTEM image (Fig. 3f) taken from the selected area of Fig. 3e shows clear lattice fringes of (113) planes ($d = 1.78$ Å), which are oriented along the extension direction of the nanowire.

XPS investigation was carried out to elucidate the valence state of the as-prepared NBT nanowires. The full survey XPS spectrum in Fig. S5† clearly shows the existence of Na, Bi, Ti and O elements in the sample. The high-resolution XPS spectrum of Na 1s (Fig. 4a) shows a peak at 1070.75 eV. Fig. 4b presents two main peaks at 158.75 and 164.05 eV, which correspond to Bi $4f_{7/2}$ and Bi $4f_{5/2}$, respectively. Fig. 4c shows the high-resolution XPS spectrum of Ti 2p. The Ti $2p_{3/2}$ and Ti $2p_{1/2}$ peaks are located at 457.9 eV and 464 eV, respectively, in accordance with the data of Ti^{4+}. The XPS spectrum of O 1s in Fig. 4d is deconvoluted into three peaks, which can be assigned to lattice oxygen (O_L, 529.2 eV), defective oxygen (O_V, 531.1 eV) and surface adsorbed oxygen (O_C, 533.8 eV), respectively.[35] The presence of oxygen vacancies could efficiently promote the adsorption and activation of O_2 on the surface of the piezocatalyst and consequently enhance piezocatalytic activity.[36] Therefore, it is speculated that the oxygen vacancy defects in NBT may contribute to its excellent piezocatalytic performance. However, the effect of oxygen defects on the energy band structure and the mechanism of improving the piezocatalytic performance need to be further studied.

PFM testing was employed to characterize the piezoelectricity of the prepared NBT nanowires. The experimental setup of PFM is illustrated in the inset of Fig. 5a. By applying a tip bias of ±3 V, localized point-to-point piezo-responses of the samples were probed. The PFM amplitude–voltage butterfly curve and phase–voltage hysteresis loop are given in Fig. 5. The butterfly-shaped curve appears symmetrical, indicating the certain piezoelectric properties. On the other hand, the phase hysteresis loop presents about 180° domain switching at ±3 V (Fig. 5b).

To study the piezocatalytic performance of NBT nanowires, diverse industrial pollutants, including anionic dyes (RhB and MB), a cationic dye (MO), and neutral stubborn pollutants (TH, BPA and phenol), are used as target contaminants. Fig. 6a–f

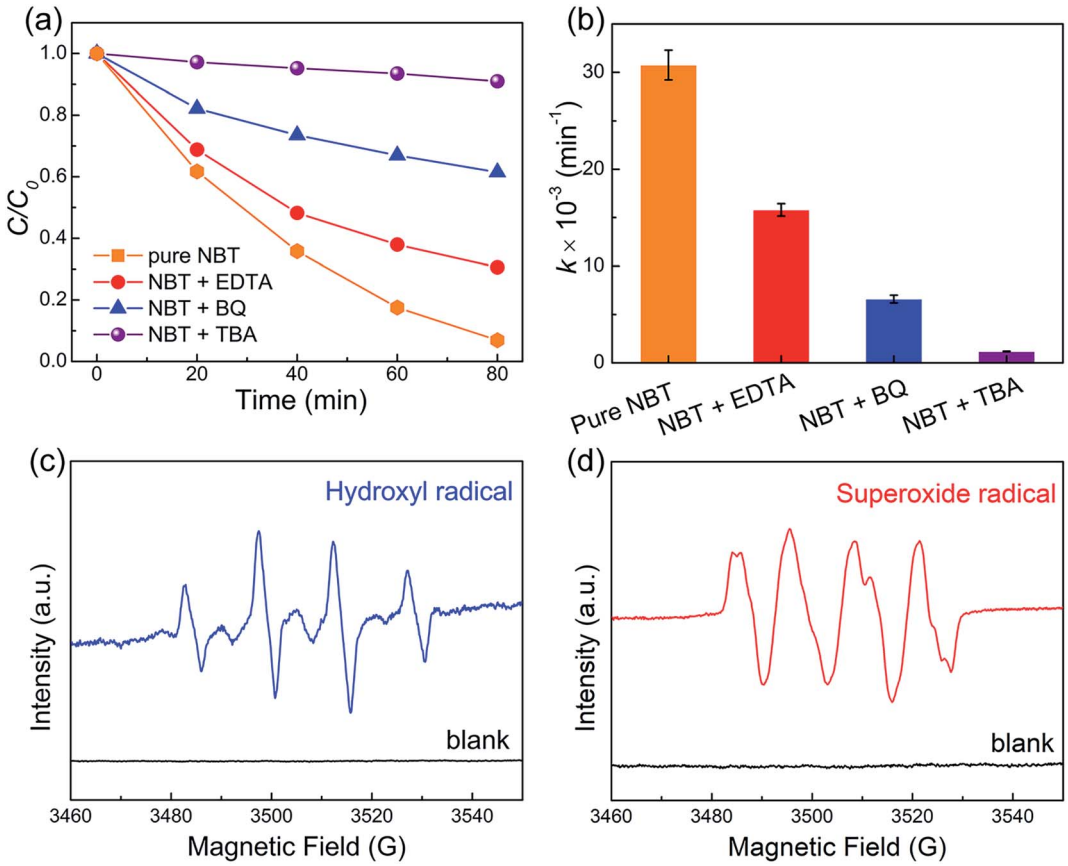

Fig. 7 (a) Active species trapping degradation experiments for $Na_{0.5}Bi_{0.5}TiO_3$ under simultaneous ultrasonic vibration in the degradation of MO, (b) corresponding first-order rate constants with various scavengers. DMPO spin-trapping ESR spectra of the (c) DMPO–·OH adduct in H_2O dispersion and (d) DMPO–$\cdot O_2^-$ adduct in DMSO dispersion of $Na_{0.5}Bi_{0.5}TiO_3$.

display the typical absorption spectra of the aqueous solutions of these pollutants. Piezocatalytic experiments without using NBT were carried out. It was clear that the pollutants could hardly be degraded without NBT under ultrasonic vibration. After being treated with ultrasonic vibration for 80 min, RhB, MO, MB, TH, BPA and phenol were removed 100%, 92.8%, 66.7%, 65.7%, 60.6% and 58.5% (Fig. 6g), respectively. The results demonstrated that the NBT nanowires are effective in degrading various kinds of organic pollutants. The first-order rate constants for the piezocatalytic degradation of the target pollutants were evaluated by refinement of the $\ln(C_0/C) - t$ plot (Fig. 6h). The results are presented in Fig. 6i. The highest rate constant (0.0575 min^{-1}) was obtained for RhB. The piezocatalytic performance of NBT samples in this work was compared with that of other reported NBT materials. As shown in Table 1, the NBT nanowires prepared by the template hydrothermal method show the highest piezocatalytic performance.

To distinguish the role of active radicals in the piezocatalytic degradation of MO over NBT, trapping experiments were conducted using TBA, BQ and EDTA–2Na as radical scavengers. As revealed in Fig. 7a and b, the piezocatalytic performance was inhibited greatly upon introducing TBA, which indicated that ·OH was the primary active species. Furthermore, the piezocatalytic oxidation ability of NBT was also restrained by the addition of BQ and EDTA, indicating that $\cdot O_2^-$ and h^+ played an auxiliary role in the piezocatalytic degradation of MO over NBT. ESR characterization was carried out to confirm the existence of ·OH and $\cdot O_2^-$. The nitrone spin trap 5,5-dimethyl-1-pyrroline N-oxide (DMPO) was introduced into the aqueous and dimethyl sulphoxide (DMSO) dispersions of the NBT catalyst for probing hydroxyl radicals (·OH) and superoxide radicals ($\cdot O_2^-$), respectively. Well-defined signals (Fig. 7c and d) of the specific DMPO–·OH and DMPO–$\cdot O_2^-$ adducts were observed after being treated with ultrasound for 5 minutes. These results confirmed the generation of ·OH and $\cdot O_2^-$ radicals in the piezocatalytic process.

Conclusions

In summary, a novel template hydrothermal reaction for the large-scale synthesis of NBT nanowires has been developed. The as-prepared NBT nanowires exhibited superior piezocatalytic performance for the degradation of various organic pollutants. Particularly, the highest degradation rate was obtained for RhB (100% in 80 min). The active species capture experiments and ESR measurements reveal that ·OH, $\cdot O_2^-$ and h^+ play important roles in the piezocatalytic process in the order of ·OH > $\cdot O_2^-$ > h^+. In view of the superior piezocatalytic performance of NBT nanowires, the template hydrothermal method developed here has great potential for large scale synthesis of other piezoelectric perovskite $ATiO_3$ nanowire nanostructures.

Conflicts of interest

The authors declare no competing financial interest.

Acknowledgements

This work was supported by the China Postdoctoral Science Foundation (2020M672959), National Natural Science Foundation of China (No. 51872335 and 51202298), and Natural Science Foundation of Guangdong Province, China (No. 2015A030311019).

References

1 F. Rudroff, M. D. Mihovilovic, H. Gröger, R. Snajdrova, H. Iding and U. T. Bornscheuer, *Nat. Catal.*, 2018, **1**, 12–22.
2 H. Tong, S. Ouyang, Y. Bi, N. Umezawa, M. Oshikiri and J. Ye, *Adv. Mater.*, 2012, **24**, 229–251.
3 J. J. Pignatello, E. Oliveros and A. MacKay, *Crit. Rev. Environ. Sci. Technol.*, 2006, **36**, 1–84.
4 L. Gomathi Devi, S. Girish Kumar, K. Mohan Reddy and C. Munikrishnappa, *J. Hazard. Mater.*, 2009, **164**, 459–467.
5 E. J. Rosenfeldt and K. G. Linden, *Environ. Sci. Technol.*, 2004, **38**, 5476–5483.
6 D. Chatterjee and S. Dasgupta, *J. Photochem. Photobiol., C*, 2005, **6**, 186–205.
7 L. Bilińska, K. Blus, M. Gmurek and S. Ledakowicz, *Chem. Eng. J.*, 2019, **358**, 992–1001.
8 H. You, Z. Wu, L. Zhang, Y. Ying, Y. Liu, L. Fei, X. Chen, Y. Jia, Y. Wang, F. Wang, S. Ju, J. Qiao, C.-H. Lam and H. Huang, *Angew. Chem., Int. Ed.*, 2019, **58**, 11779–11784.
9 S. Tu, Y. Guo, Y. Zhang, C. Hu, T. Zhang, T. Ma and H. Huang, *Adv. Funct. Mater.*, 2020, **30**, 2005158.
10 J. Wu, Q. Xu, E. Lin, B. Yuan, N. Qin, S. K. Thatikonda and D. Bao, *ACS Appl. Mater. Interfaces*, 2018, **10**, 17842–17849.
11 T. P. Pham Thi, Z. Yan, G. Nick, K. Hamideh, H. D. Nguyen Phuc, Z. Xuefan, Z. Dou, Z. Kechao, D. Steve and B. Chris, *Iscience*, 2020, **23**, 101095.
12 B. Yuan, J. Wu, N. Qin, E. Lin, Z. Kang and D. Bao, *Applied Materials Today*, 2019, **17**, 183–192.
13 Z. Kang, N. Qin, E. Lin, J. Wu, B. Yuan and D. Bao, *J. Cleaner Prod.*, 2020, **261**, 121125.
14 D. Yu, Z. Liu, J. Zhang, S. Li, Z. Zhao, L. Zhu, W. Liu, Y. Lin, H. Liu and Z. Zhang, *Nano Energy*, 2019, **58**, 695–705.
15 S. Singh and N. Khare, *Nano Energy*, 2017, **38**, 335–341.
16 L. Guo, C. Wang, X. Luo, G. Cui and H. Li, *Chem. Commun.*, 2010, **46**, 5960–5962.
17 O. Y. Podyacheva and Z. R. Ismagilov, *Catal. Today*, 2015, **249**, 12–22.
18 Y. Zhang, T. Mori, J. Ye and M. Antonietti, *J. Am. Chem. Soc.*, 2010, **132**, 6294–6295.
19 D. Voiry, J. Yang and M. Chhowalla, *Adv. Mater.*, 2016, **28**, 6197–6206.
20 Z. Zhao, L. Wei, S. Li, L. Zhu, Y. Su, Y. Liu, Y. Bu, Y. Lin, W. Liu and Z. Zhang, *J. Mater. Chem. A*, 2020, **8**, 16238–16245.
21 B. K. Barick, R. N. P. Choudhary and D. K. Pradhan, *Mater. Chem. Phys.*, 2012, **132**, 1007–1014.
22 X. Liu and X. Tan, *Adv. Mater.*, 2016, **28**, 574–578.
23 P. Marchet, E. Boucher, V. Dorcet and J. P. Mercurio, *J. Eur. Ceram. Soc.*, 2006, **26**, 3037–3041.

24 R. Zhang, X. Wu, Y. Li, W. Shao, Y. Zhang, Z. Liu, J. Nie, J. Tan and W. Ye, *RSC Adv.*, 2020, **10**, 7443–7451.
25 D. Liu, Y. Song, Z. Xin, G. Liu, C. Jin and F. Shan, *Nano Energy*, 2019, **65**, 104024.
26 G. Cilaveni, K. V. Ashok Kumar, S. S. K. Raavi, C. Subrahmanyam and S. Asthana, *J. Alloys Compd.*, 2019, **798**, 540–552.
27 Y. Zhang, W. Fu, H. Yang, M. Li, Y. Li, W. Zhao, P. Sun, M. Yuan, D. Ma, B. Liu and G. Zou, *Sens. Actuators, B*, 2008, **135**, 317–321.
28 Y. Liu, Y. Lu and S. Dai, *J. Alloys Compd.*, 2009, **484**, 801–805.
29 H. Zhang, L. Liu, M. Zhu, Y. Hou, R. Wang and H. Yan, *Int. J. Appl. Ceram. Technol.*, 2016, **13**, 569–578.
30 H. Xu, L. Gao and J. Guo, *J. Am. Ceram. Soc.*, 2002, **85**, 727–729.
31 N. Bao, L. Shen, G. Srinivasan, K. Yanagisawa and A. Gupta, *J. Phys. Chem. C*, 2008, **112**, 8634–8642.
32 A. Rudola, K. Saravanan, C. W. Mason and P. Balaya, *J. Mater. Chem. A*, 2013, **1**, 2653–2662.
33 J. Wu, N. Qin, E. Lin, B. Yuan, Z. Kang and D. Bao, *Nanoscale*, 2019, **11**, 21128–21136.
34 G. Xu, Y. Yang, H. Bai, J. Wang, H. Tian, R. Zhao, X. Wei, X. Yang and G. Han, *CrystEngComm*, 2016, **18**, 2268–2274.
35 K. K. Bharathi, B. Moorthy, H. K. Dara, L. Durai and D. K. Kim, *J. Mater. Sci.*, 2019, **54**, 13236–13246.
36 P. L. Wang, X. Y. Li, S. Y. Fan, X. Chen, M. C. Qin, D. Long, M. O. Tad and S. M. Liu, *Appl. Catal., B*, 2020, **279**, 119340.
37 R. Zhang, X. Wu, Y. Li, W. Shao, Y. Zhang, Z. Liu, J. Nie, J. Tan and W. Ye, *RSC Adv.*, 2020, **10**, 7443–7451.
38 D. Liu, Y. Song, Z. Xin, G. Liu, C. Jin and F. Shan, *Nano Energy*, 2019, **65**, 104024.